



## Research article

# Thin film liquid-vapor phase change phenomena over nano-porous substrates: A molecular dynamics perspective

Md. Aminul Islam, Monoranjan Debnath Rony, Mohammad Nasim Hasan \*

*Department of Mechanical Engineering, Bangladesh University of Engineering and Technology (BUET), Dhaka, 1000, Bangladesh*

## ARTICLE INFO

**Keywords:**

Nano porous substrate  
Molecular dynamics  
Thin film evaporation  
Self-diffusion coefficient

## ABSTRACT

Surfaces with nano-pores have significant effect in enhancing heat transfer during phase change process. In this study, Molecular dynamics simulations have been performed to investigate thin film evaporation over different nano-porous substrate. The molecular system consists of argon as the working fluid and Platinum as the solid substrate. To study the effect of the nano-pores in phase change process, the nano-porous substrates had been structured with four different hexagonal porosity with three different heights. The structures of the hexagonal nano-pore were characterized through variation of void fraction as well as height to arm thickness ratio. Qualitative heat transfer performance has been characterized by closely monitoring the temporal variation of temperature and pressure, net evaporation number, wall heat flux of the system for all cases under consideration. The quantitative characterization of heat and mass transfer performance has been done by calculating the average heat flux and evaporative mass flux. Diffusion coefficient of argon is also evaluated to illustrate the effect of these nano-porous substrate in enhancing the movement of argon atoms thus heat transfer. It has been found that the presence of hexagonal nano-porous substrates significantly increases heat transfer performance. Structures with lower void fraction offers better enhancement of heat flux and other transport characteristics. Increment in nano-pores height also significantly enhances heat transfer. Present study clearly points out the noteworthy role associated with nano-porous substrate in modulating heat transfer characteristics during liquid-vapor phase change phenomena both from qualitative and quantitative perspectives.

## 1. Introduction

Phase change phenomena has long been an area of interest for researchers of various field. Specifically, nanoscale thin-film evaporative phase change is studied extensively in the recent times. The conventional single-phase heat transfer is falling behind to full-fill the ever-increasing energy transport performance demand, whereas evaporative phase change system has the potential to transfer a huge amount of energy with a relatively small temperature variation at a smaller space. Thus, this concept is used in many engineering applications in recent times such as, thermal management of undersized components used in various technologies [1], for the cooling of sensitive micro and nano-electric devices, ultra-thin pipes, etc [2–5]. As devices get smaller, increasing heat transfer capability is necessary for optimized performance. Refrigeration, cryogenics, colloidal deposition on a solid [6], jet impingement quenching [7], microfluidic device cooling [8], and so on are some of the few cases where phase change is implied.

\* Corresponding author.

E-mail address: [nasim@me.buet.ac.bd](mailto:nasim@me.buet.ac.bd) (M.N. Hasan).

<https://doi.org/10.1016/j.heliyon.2023.e15714>

Received 6 October 2022; Received in revised form 12 April 2023; Accepted 19 April 2023

Available online 27 April 2023

2405-8440/© 2023 The Authors. Published by Elsevier Ltd. This is an open access article under the CC BY-NC-ND license (<http://creativecommons.org/licenses/by-nc-nd/4.0/>).

Nanoscale surface modification such as nanostructured and nano porous surfaces can enhance boiling heat transfer [9]. Among all of such modification, porous surfaces are of particular importance in micro/nano engineered surfaces because they can significantly improve evaporative or boiling heat transfer [10–12]. In recent times, several experimental studies have proven the effectiveness of heat transfer through porous medium [13,14]. The study of phase transition through porous surfaces will enable us to understand various natural phenomenon as these types of surfaces are quite common in nature. Mori et al. [13] revealed that the capillary action through a honeycomb porous plate can contribute to enhance the critical heat flux (CHF) and the height of the porous medium can change the outcome. They showed that attachment of Honeycomb shaped porous plate enhanced critical heat flux (CHF) approximately 2.5 times compared to flat surface in case of saturated pool boiling. Khan et al. [14] also showed the effectiveness of a 2D modulated micro-porous surface to enhance system performance. Nanoparticle coating on some selected locations can enhance the performance significantly. Mesh-covered surfaces have similar structure to porous surfaces, and Li et al. [15] showed that, both mesh size and porosity are the parameters that effects heat transfer coefficient, but evaporation or boiling inception is strongly dependent on

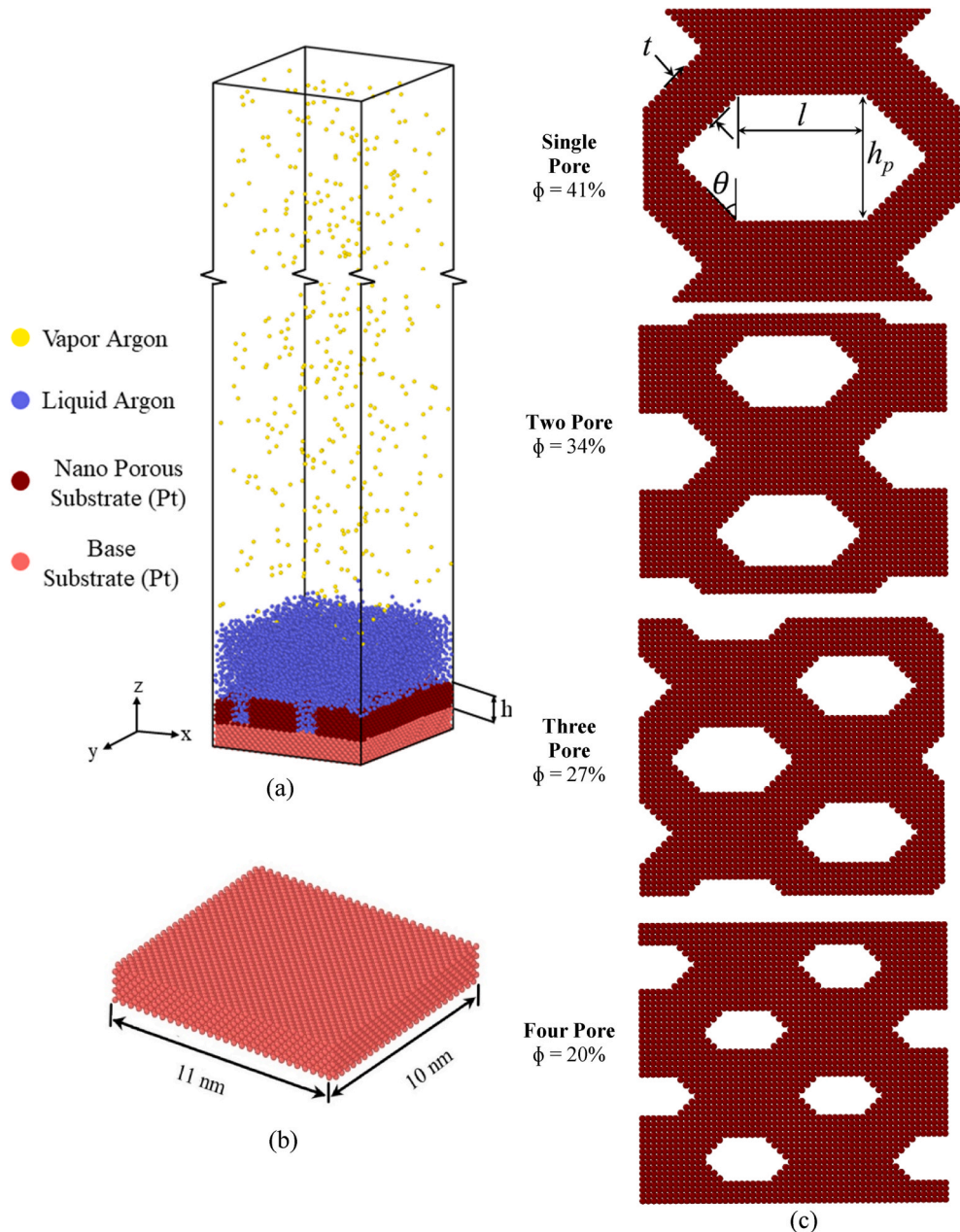


**Fig. 1.** (a) Initial Configuration of the simulation domain (11 nm (x) x 10 nm (y) x 100 nm (z)) (b) Base Substrate (Pt wall) (c) Top View of different nano-porous substrate configuration.

mesh size and weakly dependent on porosity. Zhang et al. [16] investigated the effect of bubble sizes on heat transmission through gradient microporous meshes and discovered that the bubbles with small diameters depart the mesh quickly. Meshes having micro or nano structures, according to Wen et al. [17], have low flow resistance and provide better film boiling supply. Dai et al. [18] studied evaporating mesh surfaces attached to the microchannels and discovered improved heat transfer owing to increased capillary pressure and lower flow resistance.

Nanofabrication techniques [19] has made it possible to fabricate nanostructured and nano porous surfaces. However, technological and resource limitation makes it difficult to experimentally understand the underlying mechanism for heat transfer enhancement in nanoengineered surfaces. In such cases Molecular Dynamics (MD) simulation is a fascinating and effective tool that considers all the physical phenomenon down to the atomic level which can contribute to find some crucial underlying mechanism. Using this MD simulation tool, some excellent studies have been done on the effect of heat transfer increment for evaporative phase change process [20–22] and especially on nanostructured surfaces [23–25]. Wang et al. [24] developed a molecular dynamics simulation with an aluminum substrate decorated with nanostructures of different heights. The simulation results indicated higher heat transfer efficiency and increment of evaporation rate with the nanostructures' height in a certain range. Cao et al. [26] studied the evaporation characteristics on sinusoidal nanostructures substrate and showed that as the nanostructure height and number increases heat transfer across the solid-liquid interface increases. Liu et al. [27] investigated the boiling heat transfer mechanism on nanostructured grooves at the nanoscale. There he concluded that, nanogroove with a maximum surface area (square shaped) can minimize the nanoscale boiling time and as the contact area increases, the interaction energy between the solid and liquid increases which enhances the heat transfer to the liquid and decreases interfacial resistance. Shavik et al. [28] simulated explosive boiling on nanostructured surfaces under different wetting conditions and showed that nanostructure height had a lesser effect on the heat transfer rate under hydrophobic surface conditions. Hu and Sun [29] investigated thin film evaporation and nucleate boiling on nanostructured surfaces, finding a peak heat transfer coefficient of  $31\text{MW/m}^2\text{K}$ . Bai et al. [30,31] analyzed explosive boiling on simple copper surfaces and discovered that raising the surface roughness ratio resulted in a larger surface area and lower Kapitza resistance, which improves boiling heat transmission. Ahmed et al. [32] investigated nanoscale boiling on mesh-covered surfaces and found that porous and simple mesh-covered surfaces increased evaporation rate by 23.89% and 19.16%, respectively compared to flat surface. Most of the simulations showed a huge heat flux transfer to fluid, such as  $480\text{MW/m}^2$  by Liu et al. [23],  $600\text{--}1000\text{MW/m}^2$  by Diaz and Guo [33] and  $1100\text{MW/m}^2$  by Shavik et al. [28].

MD simulations of phase change process over different innovative nanostructured surfaces are being carried out till today, but most of the studies are concerned with nanostructures such as nanopillars, nanochannels. Literature observations shows very little concern about hexagonal honeycomb nano-porous substrates for thin-film liquid evaporation. To the best of author's knowledge, no MD study has been conducted yet, to analyze evaporation and diffusion characteristics over nano porous substrate with hexagonal nano pores. So, using nonequilibrium molecular dynamics simulations, we explored the evaporative heat transfer mechanism and diffusion of liquid Argon across a platinum hexagonal nano porous substrate throughout this literature. Nano porous substrate of twelve different configuration altering their void fraction and height is investigated in this study to understand how nano porous substrate influence evaporative heat transfer process.

## 2. Methodology

The modeling of Molecular Dynamics (MD) simulation of our phase change process started by defining void fraction ( $\phi$ ) and height to arm thickness ( $\lambda$ ) ratio to distinguish between our nanostructures. Using a computational molecular dynamics simulation tool, we modeled and simulated our system which is described elaborately in the following subsections.

### 2.1. Simulation domain and interatomic potential

In this present study, Molecular dynamics simulation have been conducted on a system consisting of a vapor argon layer over a liquid argon layer which sits in top of a nano porous platinum substrate as shown in Fig. 1(a) and Fig. 1(b). Dimension of the simulation box is  $11\text{ nm (x)} \times 10\text{ nm (y)} \times 100\text{ nm (z)}$  where the z-dimension has been kept large enough to eliminate the influence of top boundary on evaporation characteristics. Periodic boundary condition is applied along both lateral (x and y) direction and fixed boundary condition in the z direction which is normal to the solid-liquid interface. A fictitious reflective wall boundary condition is also applied at the top wall of the simulation domain to prevent the loss of vapor atom and hence energy. The flat base is composed of solid platinum atoms which is  $1.5\text{ nm}$  thick and are arranged in a face centered cubic (FCC) lattice structure with a lattice constant of  $3.92\text{ \AA}$ . Total 8 layers of platinum atoms is placed at the base above which the nano porous substrate is placed where each layer consists of 1428 platinum atoms. The bottom two layers of the platinum atoms is kept fixed to prevent the loss of platinum atoms and distortion of the base. The temperature of the adjacent two layers is maintained using a thermostat, as they act as a heat source in the simulation system. The remaining four layers work as conduction layers transferring heat from the heat source to the liquid argon atoms. Initial thickness of the liquid layer put on top of the solid substrate was  $5\text{ nm}$  in all cases. As liquid layer thickness was kept constant for all cases, so the number of liquid argon atoms were different for different nano porous substrates. The Nano-porous substrate is kept submerged in the liquid argon layer. The rest of the domain is occupied by vapor argon atoms.

Nano porous substrate with four different configuration and each having three different height is considered in this study which is shown in Fig. 1(c). The substrates having hexagonal shaped nano pores are differentiated using void fraction ( $\phi$ ) which is defined as (1):

$$\phi = \frac{\text{Pore Volume}}{\text{Total Volume of the nano porous substrate}} \times 100 \% \quad (1)$$

The four nano-porous substrates had one, two, three and four hexagonal nano pores respectively. The value of  $\phi$  for the four substrates are 41%, 34%, 27% and 20% respectively. Two parameters are used to define the nano porous substrate which are arm thickness ( $t$ ) and substrate height ( $h$ ) as shown in Fig. 1(a). Substrate height ( $h$ ) is the thickness of the nano porous substrate in the z-direction. Also, several other parameters are used to define the nano pore size which are presented in Table 1. The height of the nano porous substrate was varied keeping the arm thickness ( $t$ ) constant at 1.801 nm. Thus, nano porous substrate of three different height to arm thickness ( $\lambda$ ) ratio (0.98, 1.5 and 2.1) was developed. The different nano porous substrate configurations are also shown in Fig. 1(c).

Although EAM [34] and MEAM [35] potentials can be used to accurately calculate the interactions between platinum (Pt) atoms, it is computationally expensive. In this study heat transfer between platinum and liquid argon was the primary focus, rather than heat transfer within the platinum wall. Lennard-Jones (LJ) potential [36] is appropriate in this respect, as demonstrated in several literatures [28,37]. So, the interaction between all the atoms in this study is described by LJ potential and a truncated form of the LJ potential is used in this study to save computational cost further which is as follows (2):

$$U_{ij} = \begin{cases} 4\epsilon_{ij} \left[ \left( \frac{\sigma_{ij}}{r_{ij}} \right)^{12} - \left( \frac{\sigma_{ij}}{r_{ij}} \right)^6 \right] & r_{ij} \leq r_c \\ 0 & r_{ij} > r_c \end{cases} \quad (2)$$

where  $r_{ij}$  is the distance between atom  $i$  and atom  $j$ ,  $\epsilon$  is the potential well depth,  $\sigma$  is the characteristic length at which the interatomic potential is zero and  $r_c$  is the cutoff distance beyond which interatomic interactions are not considered. The values of interatomic potential parameters are listed in Table 2, which are based on the work of Yu et al. [38]. Hasan et al. [39] showed that cut-off radius beyond  $4 \sigma_{\text{Ar-Ar}}$  (1.36 nm) has no significant impact on the simulations result, so, it was chosen as the cut-off radius in our study. Analytical tail correction was also not considered in our study to improve computational efficiency.

## 2.2. Simulation procedure

In case of each simulation prior to the thin-film phase transition, equilibration of the system is done using NVE ensemble to minimize the system energy. Duration of the total equilibration period was 2 ns and to equilibrate the system at 90 K temperature, Langevin thermostat is set at 90 K for the first 1 ns and then the entire system is allowed to equilibrate for the next 1 ns without Langevin thermostat. After the equilibration period some Pt atoms are quickly heated up to 160 K temperature using the Langevin thermostat which acts as a heating source and initiate the phase change of liquid argon layer over the nano porous substrate. The entire system is then monitored for the next 4 ns with the NVE ensemble. Throughout this study time integration is carried out by Velocity-Verlet algorithm to calculate atom propagation. Fig. 2 shows simulation results for timestep of 1, 3 and 5 fs. From the figure it is seen that the results don't vary significantly for these timesteps. So, to save computational cost timestep of 5 fs is chosen for this study. Large-scale Atomic/Molecular Massively Parallel Simulator (LAMMPS) [40] was used to carry out the simulations and OVITO [41] was used for visualization.

## 2.3. Equilibrium characteristics and model validation

To check whether the system is in equilibrium state or not after the initial equilibration period of 2 ns, spatial density of argon along the normal direction of solid surface is monitored at different instants. Fig. 3 shows the density variation of argon along z direction for the case of single nano pore substrate ( $\phi = 41\%$ ) at four instants during the equilibration period. It is visible from the figure that the

**Table 1**  
Characteristic dimension for nano porous substrates as illustrated in Fig. 1

Nano Porous Substrate	Void Fraction, $\phi$ (%)	Pore Length $l$ (nm)	Pore Width $h_p$ (nm)	Arm Thickness, $t$ (nm)	Arm Angle, $\Theta$ ( $^\circ$ )	Height to arm thickness ratio, $\lambda$
Single Pore	41	4.312	4.312	1.801	45	0.98
						1.5
						2
Two Pore	34	2.744	2.744	1.801	45	0.98
						1.5
						2
Three Pore	27	2.352	2.352	1.801	45	0.98
						1.5
						2.1
Four Pore	20	1.568	1.568	1.801	45	0.98
						1.5
						2

**Table 2**  
L-J interaction potential parameters.

Particles $i, j$	$\epsilon_{ij}$ , eV	$\sigma_{ij}$ , Å
Ar–Ar	0.0104	3.400
Pt–Pt	0.5200	2.475
Ar–Pt	0.0204	2.870

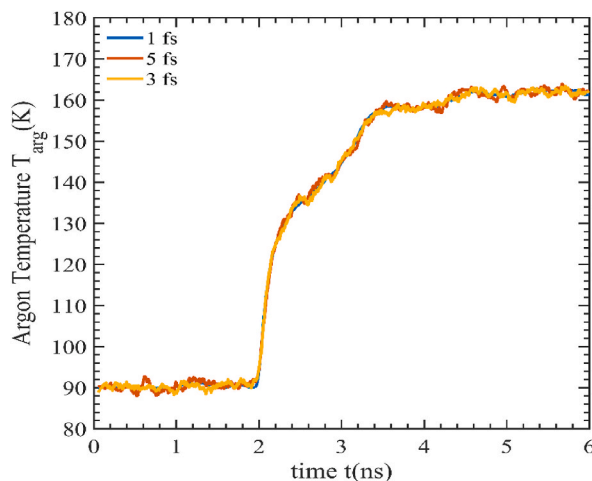


**Fig. 2.** Temporal variation of Argon temperature for different values of simulation timestep at  $\phi = 41\%$  and  $\lambda = 0.98$ .

density profile of argon is almost unchanged for all instants, indicating equilibrium state of the argon system. From the temporal variation of the total system energy for nano porous substrate of 41% void ratio ( $\phi$ ) in Fig. 4, we can further verify our system equilibration. It is apparent that the total system energy remains constant up to 2ns which indicates the system is in thermal equilibrium. The rapid increase in system energy indicates the start of evaporation period and the system energy again becomes constant as evaporation ceases.

At the end of the equilibration state, the average density of liquid argon at 90 K in this MD simulation is  $1366 \text{ kg/m}^3$  which is close to the argon density of  $1379 \text{ kg/m}^3$  reported experimentally at 90 K [42]. The similarity between the values validates the present simulation model.

### 3. Results and discussion

Findings from the simulations are presented and discussed in this section. The results are analyzed qualitatively using the atomic distribution of argon atoms over the porous substrate and by the evaporation characteristics of argon atoms. Quantitative analysis is

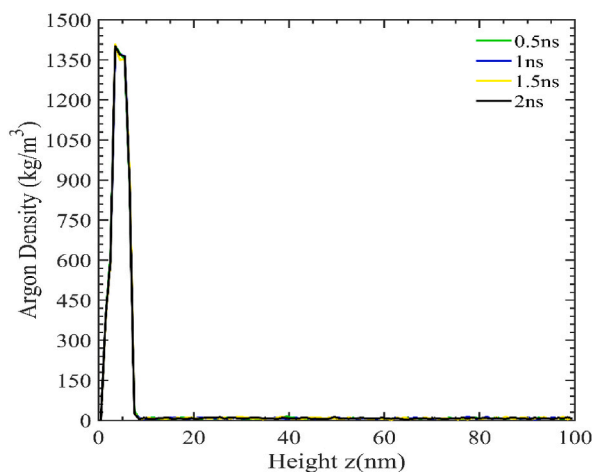


**Fig. 3.** Spatial Variation of Argon density along z-direction at different instants for single nano pore substrate ( $\phi = 41\%$ ).

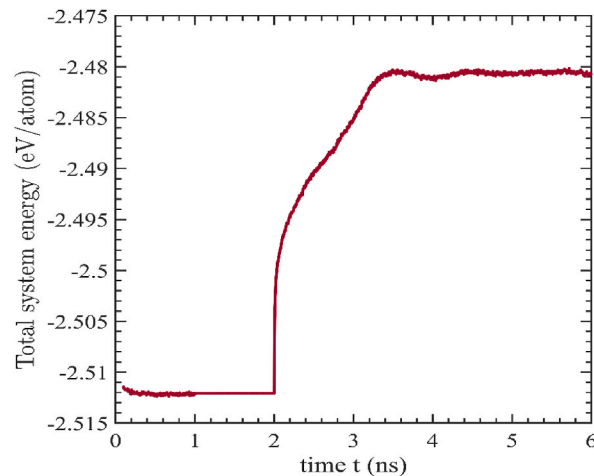


Fig. 4. Temporal Variation of Total system energy for single nano pore substrate ( $\phi = 41\%$ ).

performed by calculating Diffusion Coefficient, Wall heat flux and Evaporative mass flux of argon. Absorption characteristics are also studied to investigate and explain the effect of porous substrate on heat transfer.

### 3.1. Atomic distribution

To study the effect of nano porous substrate on thin film phase change process of liquid argon, nano porous substrate with four different void ratios has been considered along with a flat surface (FS) as reference. Snapshots of the simulation domain at specific time intervals for different void ratio ( $\phi$ ) substrate at  $\lambda = 0.98$  is presented in Fig. 5. The figure shows the comparative difference in the evolution of evaporation for different nano porous substrates with varying  $\phi$  at a constant height. For all cases, at the start of the evaporation period, there is no significant visible transition of argon from liquid to vapor phase. In flat surface, there is a significant reduction of liquid argon atoms between 3.5 and 4 ns, for nano porous substrate with  $\phi = 41\%$ , it is between 3 and 3.5 ns and for  $\phi = 20\%$  the change is between 2.75 and 3 ns. The difference in atomic distribution between the nano porous substrates is more prominent for  $t = 3$  ns. The amount of remaining non-evaporated argon atoms is maximum for  $\phi = 41\%$  and minimum for  $\phi = 20\%$ . This indicates lower  $\phi$  leads to faster evaporation.

Figs. 6 and 7 illustrate the effect of height to arm thickness ratio ( $\lambda$ ) of the nano porous substrate on atomic distribution during the evaporation process. Fig. 6 displays the snapshot of the simulation domain for  $\phi = 41\%$  at three different  $\lambda$  whereas Fig. 7 represents the snapshots for  $\phi = 20\%$ . As for  $\phi = 34\%$  and  $\phi = 27\%$  the trend of the snapshots at different  $\lambda$  is similar, we have compared the snapshots for only two values of  $\phi$ .

In both cases when  $\lambda = 2$ , the change of liquid thickness is very subtle. As increase in height leads to higher heat transfer area, in both figures, the liquid argon layer decreases more rapidly as the height of the nano porous substrate increases.

With the progress of time, thickness of the liquid argon layer decreases as sufficient heat transfer takes place between the solid substrate and the liquid argon layer in all the cases. This indicates enhancement of heat transfer by the presence of nano porous substrate.

Phase change phenomenon like boiling in such nano porous substrate and the increment of heat transfer can easily be explained with more details using both diffusion, evaporation characteristics which led us to an extensive study of these two properties.

### 3.2. Evaporation characteristics

Evaporation characteristic of the system is assessed by calculating the net evaporation number ( $N_{\text{evap}}$ ). To evaluate the net evaporation number, vapor atoms must be properly identified first. Vapor atom has been distinguished by analyzing the number of neighboring atoms around an atom. An argon atom has been counted as vapor if it has less than seven neighboring atoms within a cutoff distance [43,44]. Initial vapor atoms refer to the number of vapor atoms calculated just after the equilibration time. The number of vapor atoms is then computed at discrete times during heating period. Subtracting the number of initial vapor atoms from the number of vapor atoms at various stages during the heating period yields the number of atoms that changed its phase from liquid to vapor. Fig. 8 shows the variation of net evaporation number ( $N_{\text{evap}}$ ) with time for nano porous substrates with different void ratio  $\phi$  and constant height to arm thickness  $\lambda = 0.98$ . The slope of each curve indicates the evaporation rate for each nano porous substrate. It is apparent from the figure that  $\phi$  significantly enhance evaporation rate. For flat surface as transfer of energy from heated source to argon molecules is only from one direction, evaporation takes place for a longer time and evaporation rate is slow. Introduction of nano porous substrate leads to higher heat transfer area and solid liquid interaction [43] which enhance heat transfer. Also due to the same reason we have higher evaporation rate as the height of the nano porous substrate is increased but the final net evaporation number is significantly reduced as seen in Fig. 9(a) and Fig. 9(b). With increased height a smaller number of liquid argons remain in the

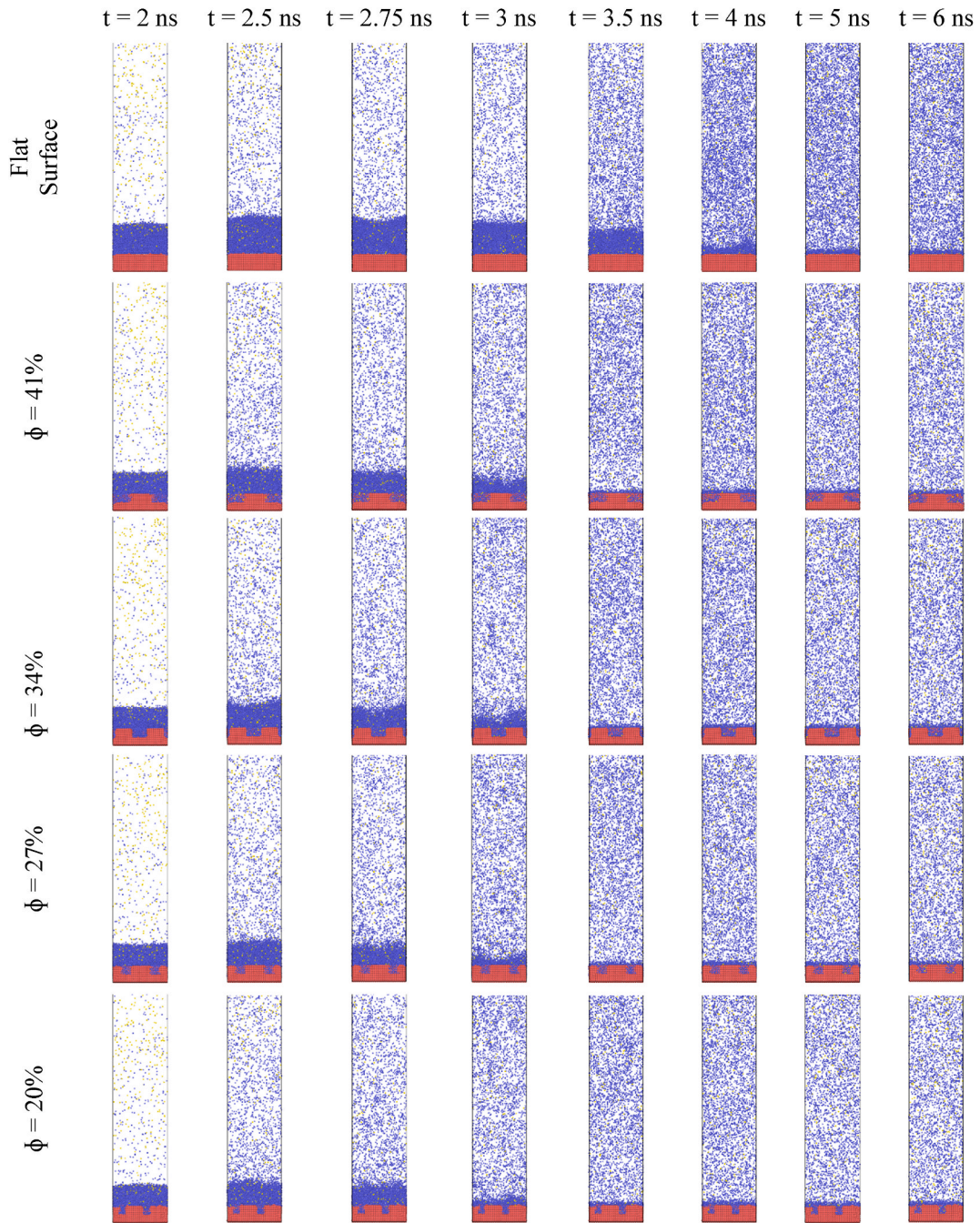


**Fig. 5.** Snapshot of the simulation domain at different time instants during the evaporation process at different void ratios ( $\phi$ ) of the nano pore substrate for  $\lambda = 0.98$ .

nano-pore thus reducing the final evaporation number. With increase in height, void volume and surface area inside the pore increases resulting in more argon atoms remaining inside of the pores. This retention of liquid atoms also significantly reduces evaporation number. So, increase of nano porous substrate height increases the binding ability of liquid atoms to the surface which is consistent with the work of Cao et al. [26]. The effect of  $\phi$  is also apparent from Fig. 9. For four nano pore substrates ( $\phi = 20\%$ ) the evaporation rate is slightly better and final net evaporation number ( $N_{\text{evap}}$ ) is lower. Although  $\phi$  is low but due to the existence of smaller pores and less retention of liquid argon atoms the evaporation rate was higher. Also for four nano pore substrates evaporation duration was short compared to single nano pore substrates.

For getting an overall view of the effect of both  $\phi$  and  $\lambda$  on evaporation characteristics, temporal variation of net evaporation number for all cases of  $\phi$  and  $\lambda$  is presented in Fig. 10. In this figure we can observe that by controlling both  $\phi$  and  $\lambda$  for the nano porous

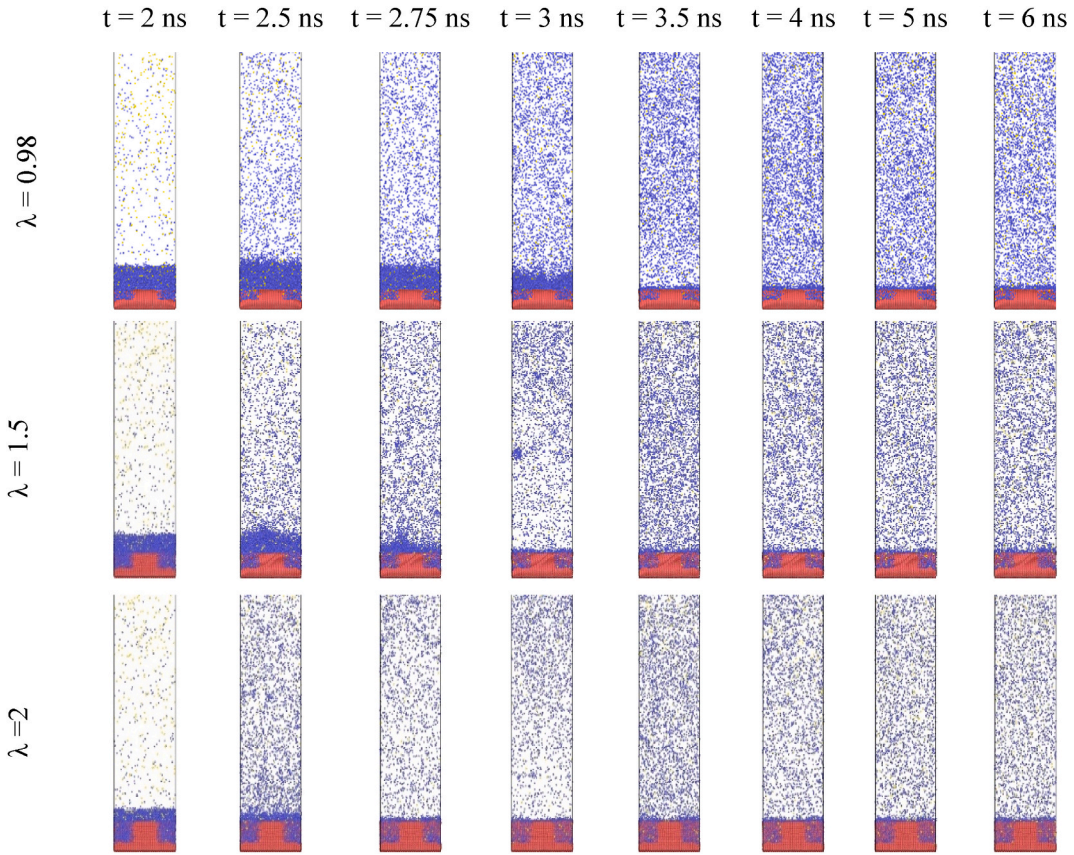


**Fig. 6.** Snapshot of the simulation domain at different time instants during the evaporation process at different heights ( $\lambda$ ) of the nano pore substrate for  $\phi = 41\%$ .

substrate we can get the desired evaporation characteristic i.e., evaporation rate and number of argon atom absorbed in the substrate. By controlling evaporation rate, we can also control the period of evaporation. This is a novel approach in modulating evaporation characteristic by changing the parameters of nano porous substrate.

Temporal variation of argon temperature is presented in Fig. 11. Similar to the net evaporation curves there is a sharp rise in the temperature of argon after 2 ns as the thermostat is switched to 160 K. Liquid argon atoms adjacent to the surface gets heated up quickly and evaporates which contribute to this sudden rise. After the initial rise the temperature drops between the time interval of 3–4 ns due to evaporation being complete and vapor having less density. The time for the drop in temperature is different for each case. At the final stage convective heat transfer takes place and the temperature of argon rises steadily and stabilizes at the end. It is observed from Fig. 11 that the rate of change of temperature is higher for nano porous substrates compared to flat surface. As the height of the nanopores increases, the time it takes to reach the initial maximum value decreases. It is due to greater heat transfer area as stated earlier. Effect of  $\phi$  is also obvious on Fig. 11, Four nano pore substrates ( $\phi = 20\%$ ) have higher rate of temperature increase and reached peak value earlier than single nano pore substrates ( $\phi = 41\%$ ). The final equilibrium temperature was less for the nano porous substrates compared to the flat surface. There were fewer liquid argon atoms in the simulation domain during the initial stage of simulation for nano porous substrates. As a result, fewer argon atoms transitioned from liquid to vapor phase at the end of the evaporation period. So, fewer vapor argon atoms were present at the end of evaporation period for nano porous substrates compared to flat substrate, resulting in a lower final temperature.

### 3.3. Diffusion characteristics

Diffusion is related to the movement of atoms. Higher diffusion of atoms indicates free and rapid movement of atoms which is useful for higher convective heat transfer. Diffusion for atoms can be quantitatively characterized by diffusion coefficient. In the present study diffusion characteristics of liquid argon is observed. For analysis Mean Square Displacement (MSD) of argon particles were evaluated using the following formula (3) according to Ref. [45]:

$$MSD(t) = \frac{1}{N} \sum_{i=1}^N \langle |r_i(t) - r_i(0)|^2 \rangle \quad (3)$$

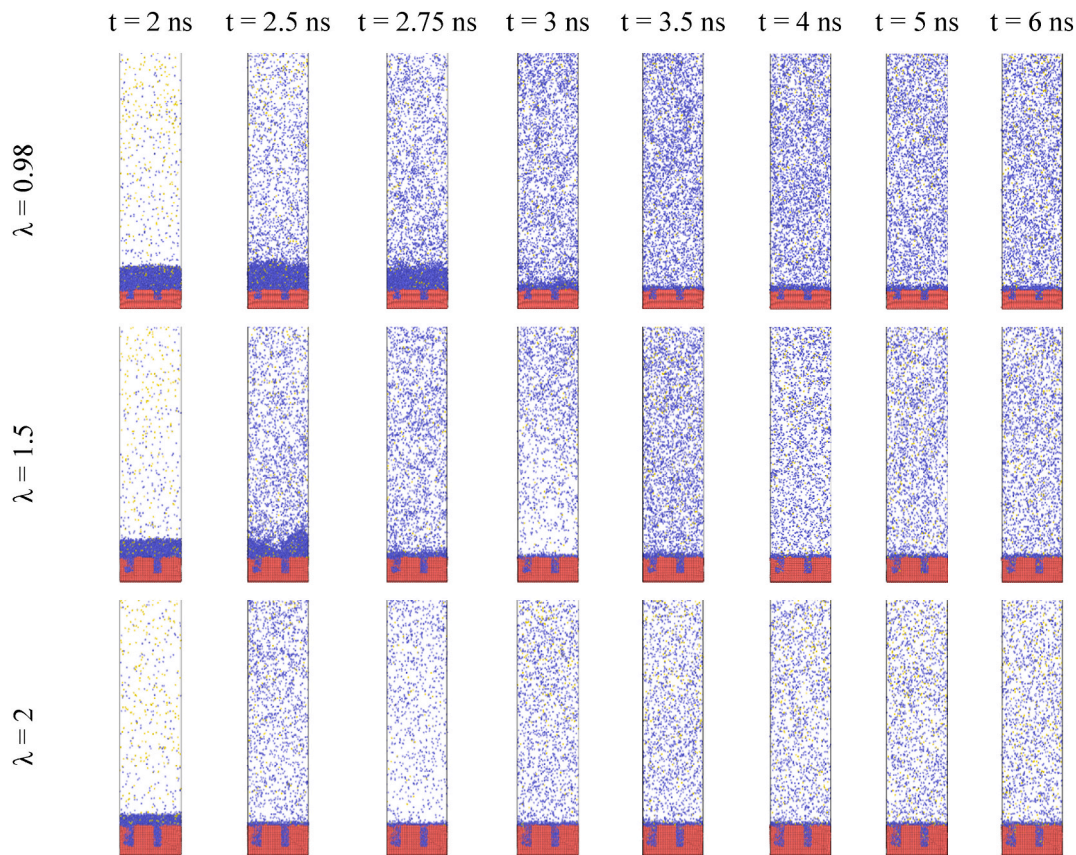


**Fig. 7.** Snapshot of the simulation domain at different time instants during the evaporation process at different heights ( $\lambda$ ) of the nano pore substrate for  $\phi = 20\%$ .

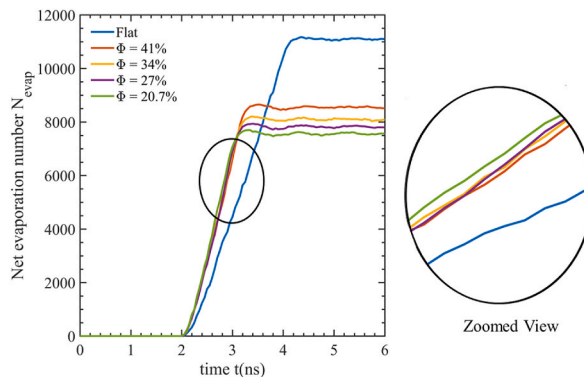


**Fig. 8.** Temporal variation of net evaporated Argon atom for different  $\phi$  at  $\lambda = 0.98$ .

here,  $r_i(t)$  and  $r_i(0)$  are the positional coordinates of  $i$ th atom at the current time and initial time respectively. And to get an understanding of how the atoms are diffused with time, MSD vs time curve for different nano porous substrates is plotted in Figs. 12 and 13. Fig. 12(a)–(d) shows the MSD plots for nano porous substrates with different  $\phi$  at  $\lambda = 0.98$  on the other hand Fig. 13(a)–(c) shows the MSD plots for different  $\lambda$  at  $\phi = 41\%$ .

All the curves are found to have similar trend, with an initial linear portion then the curve oscillates around a final value. The linear portion indicates the time up to which evaporation takes place and there is rapid movement of argon atoms during this interval. With decrease in  $\phi$  and increase in height the linear portion of the MSD curves became steeper indicating rapid increase in movement of argon atoms thus faster evaporation. Faster evaporation was also evident from the fact that curves became flat earlier. Self-diffusion coefficient ( $D$ ) is related to limiting slope of  $MSD(t)$  by the following formula (4) referencing to Ref. [45]:

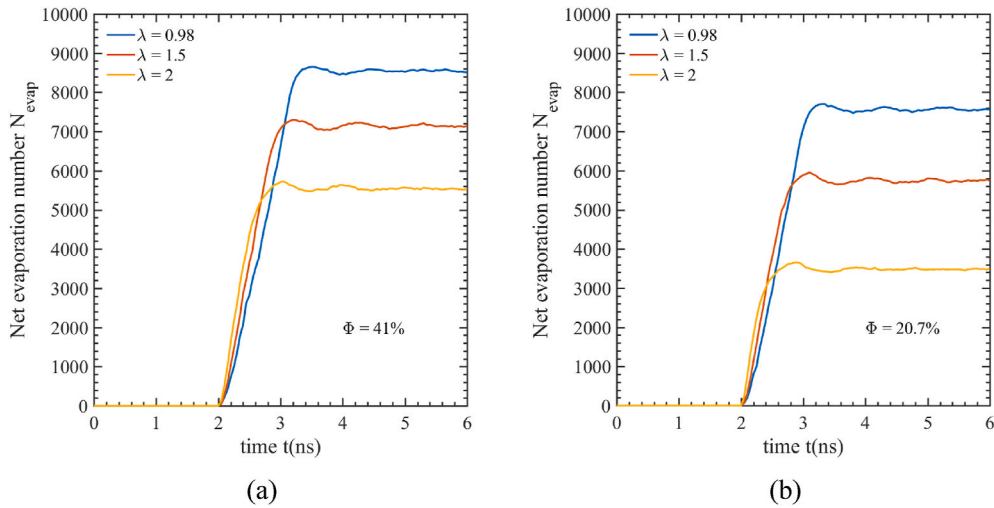


Fig. 9. Temporal variation of net evaporated Argon atom for different  $\lambda$  at (a)  $\phi = 41\%$  (b)  $\phi = 20\%$ .

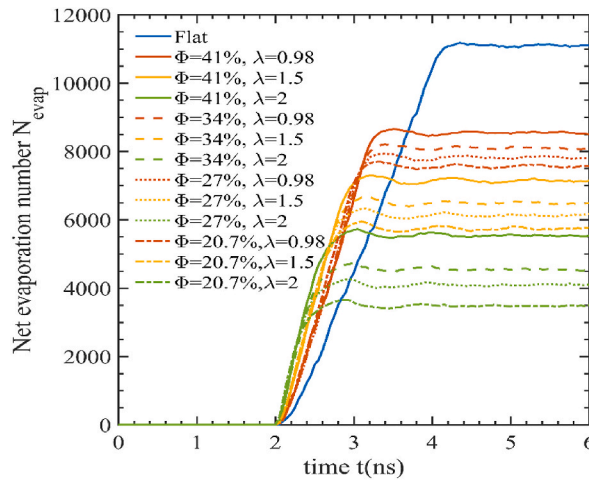


Fig. 10. Temporal variation of net evaporated Argon atom for all cases of  $\phi$  and  $\lambda$

$$D = \frac{1}{6} \lim_{t \rightarrow \infty} \frac{d(MSD(t))}{dt} \tag{4}$$

The initial portion of MSD(t) curve is linear in this study, 1/6th of the slope of the linear portion is taken to calculate self-diffusion coefficient.

Self-diffusion coefficient of argon is also significantly influenced by nano pores as seen from Fig. 14. Rapid heat transfer causes faster evaporation thus rapid movement of argon atoms. Therefore, diffusion coefficient increases as  $\phi$  of the nano porous substrate is decreased. Retention of liquids inside of the pores restricted movement of atoms inside the pore which may be one of the reasons for lower diffusion coefficient of argon for single nano pore substrate. With the height of substrate, diffusion coefficient is also observed to be increased. The increase in diffusion coefficient with height showed a linear trend. It is due to the enhancement of heat transfer area overcoming the effect of retention. The trend of self-diffusion coefficient of argon is consistent with that found from temperature, and heat flux curves.

### 3.4. Wall heat flux

Transport parameters such as wall heat flux ( $q_w$ ) and evaporative mass flux can be used to further quantify the thermal performance of the nano porous substrate. Throughout this investigation, from per atom potential energy, per atom kinetic energy, and per atom stress tensor, we computed heat flux vector,  $J$  using the following formula (5):

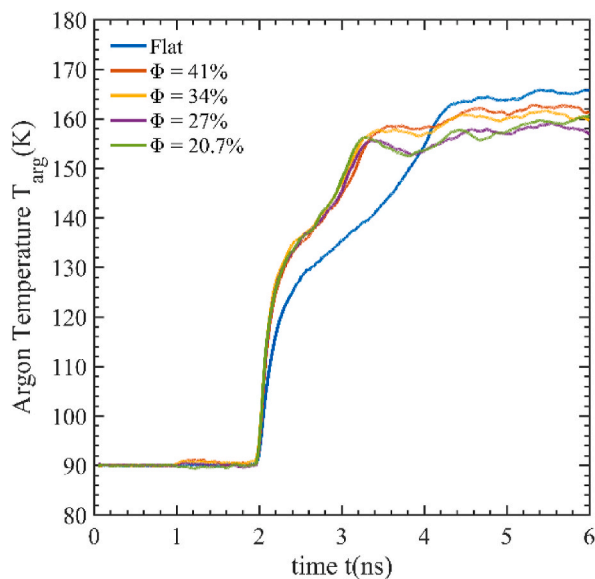


Fig. 11. Temporal variation of Argon temperature for different values of  $\phi$  with  $\lambda = 0.98$ .

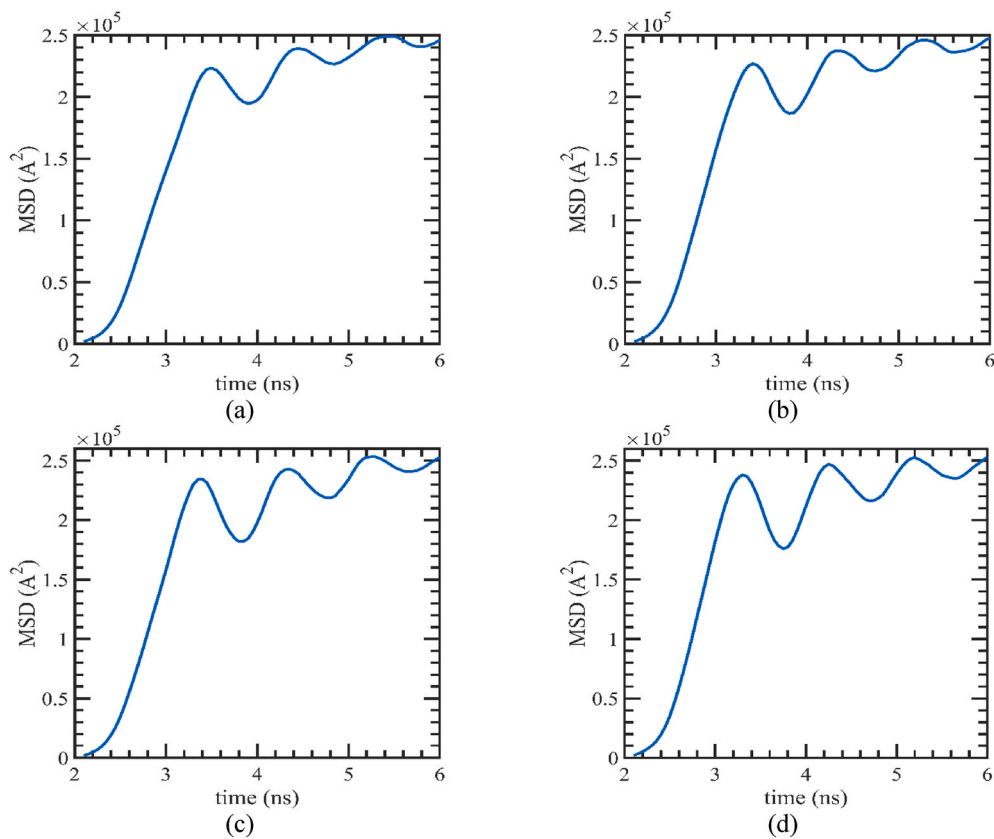


Fig. 12. Temporal variation of Mean Square Displacement (MSD) of Argon atoms for (a)  $\phi = 41\%$ , (b)  $\phi = 34\%$ , (c)  $\phi = 27\%$ , (d)  $\phi = 20\%$  for  $\lambda = 0.98$ .

$$J = \frac{1}{V} \left( \sum_i e_i v_i - \sum_i S_i v_i \right) \quad (5)$$

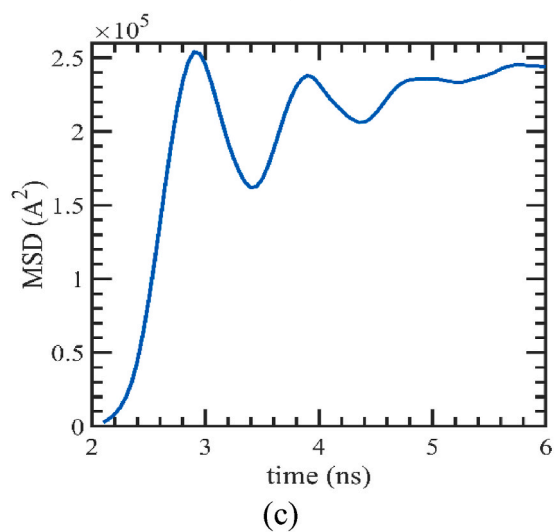
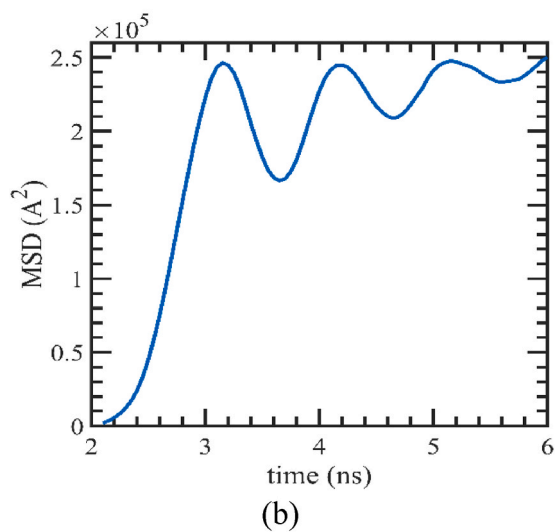
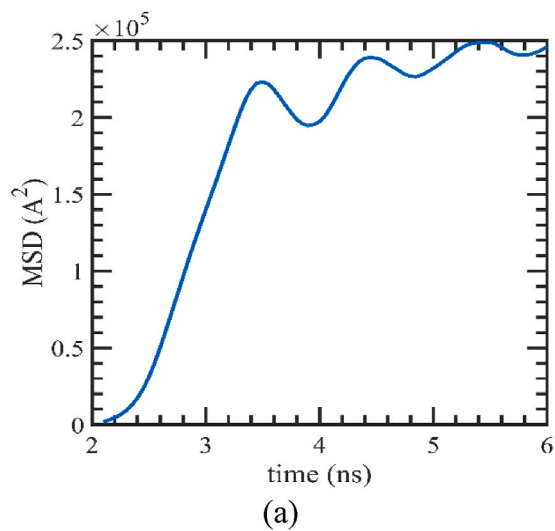


Fig. 13. Temporal variation of Mean Square Displacement (MSD) of Argon with Time for (a)  $\lambda = 0.98$ , (b)  $\lambda = 1.5$ , (c)  $\lambda = 2$  for  $\phi = 41\%$ .

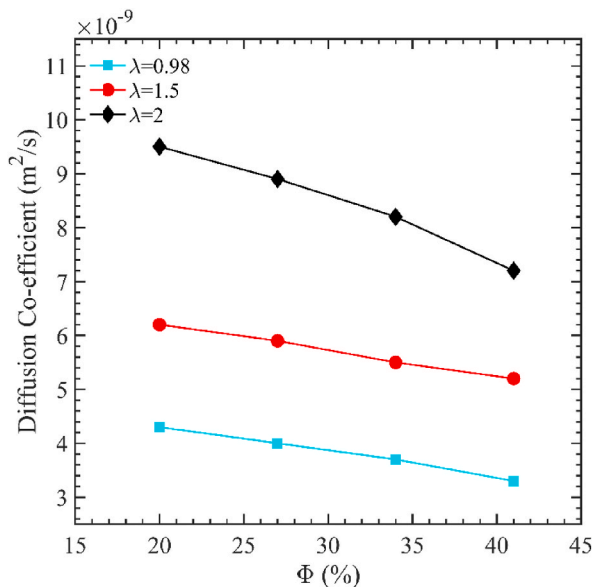


Fig. 14. Variation of Diffusion Coefficient with height void ratio ϕ of the nano porous substrate.

Component of the heat flux vector,  $J$  in the direction normal to the solid substrate ( $xy$  plane) is considered as wall heat flux throughout this study.

The fluctuation in wall heat flow over time for various nano porous substrates is shown in Fig. 15. As the thermostat temperature is changed from 90 K to 160 K, the value of heat flux reaches its maximum value. This substantial heat flux is caused by the large difference in temperature between the metal surface and the argon atoms. As evaporation progresses, the difference in temperature between the metal substrate surface and the argon diminishes, lowering the heat flux until it oscillates around zero when evaporation is complete. Fig. 15(a) shows the variation of wall heat flux for different values of ϕ at λ = 0.98. It can be seen from the figure that the magnitude of maximum heat flux is highest for nano porous substrate with ϕ = 20% and lowest for the flat surface. Higher heat flux indicates presence of more pores i.e., lower void ratio enhances heat transfer due to the increment of heat transfer area as the number of pores is increased although ϕ is less. Higher contact area increases the solid liquid interaction which resulted in higher maximum heat flux at the start of heating period. Another effect that might have influenced the heat transfer characteristics is the retention of argon inside of the pores. The nano porous substrates with ϕ = 41% have greater void volume which results in higher retention of argon, which led to less argon atom available for evaporation. Less argon taking part in evaporation led to lower heat transfer from the solid to liquid thus lowering maximum heat flux.

Height of the substrates also influences heat flux characteristics. From Fig. 15(b) it can be observed that increase in λ ratio, results in

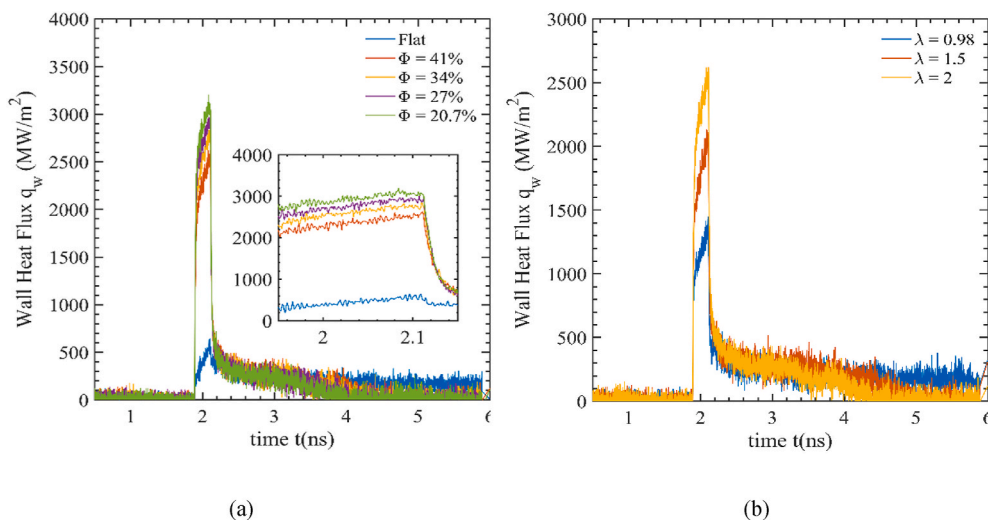


Fig. 15. Temporal variation of Wall heat flux (a) For different values of ϕ at λ = 2 (b) For different values of λ at ϕ = 41%.

higher maximum heat flux. The enhancement is due to higher heat transfer area. Unlike nano structures, there are closed void in the nano porous substrate which can trap liquid argon atoms and thus hinder the phase change phenomena. So, if the height of the nano porous substrate is increased too much it can overshadow the effect created due to higher heat transfer area. Quantitative analysis of the wall heat flux can illustrate this effect clearly.

The following equation is used to compute the time-averaged wall heat flux ( $q_{w,avg}$ ) (6):

$$q_{w,avg} = \frac{1}{t_f - t_o} \int_{t_o}^{t_f} q_w dt \quad (6)$$

Evaporation period started at 2 ns ( $t_o$ ) for all nano porous substrates, and the end time ( $t_f$ ) was different for each nanostructure. The values of time-averaged heat flux are tabulated in Table 3. For nano porous substrates average heat flux is significantly higher than the flat substrate. Introduction of single pore ( $\phi = 41\%$ ) and four pore ( $\phi = 20\%$ ) nano porous substrate increased the average heat flux by 47.1% and 68.8% respectively. Average heat flux also increased when the height of the nano porous substrate was increased. If we take the case of nano porous substrate of void ratio  $\phi = 41\%$  as an example, it is observed that when  $\lambda$  was increased from 0.98 to 1.5 average heat flux increased by 26.6%. But when  $\lambda$  was increased from 1.5 to 2 the increment was only 13%. So, even though the increase in surface area was similar the increase in average heat flux was quite different. This can be explained by the retention of argon atoms inside the pores when height of the nano porous substrate is increased too much. Increase in height of the nano porous substrate means increase in void volume and more argon atom being trapped inside of the pores contributing to less evaporation number. So, the absorption of argon atoms offset the effect of higher heat transfer area. As a result, the value of average heat flux was slightly less.

### 3.5. Absorption characteristics

From the snapshot of the simulation domain at different time intervals during the evaporation process (Figs. 5–7), we can observe that the pores do not dry out during the simulation time span which is consistent with previous studies [32,46]. Although evaporation is complete, there are always some liquid argon atoms which remains inside the pores. Fig. 16(a)-(d) shows snapshots of the pores of different nano porous substrate at the termination of simulation. Upon examining Fig. 16 and Table 4 it is observed that single nano pore substrates having higher void fraction ( $\phi = 41\%$ ), retain around 10% more argon atoms compared to four pore substrates ( $\phi = 20\%$ ).

Thus, more retention for single nano pore substrates ( $\phi = 41\%$ ) hinders heat transfer as seen earlier in evaporation and diffusion characteristics. With the increment of nano porous substrate height, void volume increases causing higher retention of argon atom inside the pores. It is also apparent from that for all cases a non-evaporating argon layer is present above the nano porous substrate. Between single and four nano-pore substrates, difference in absorption becomes the key characteristic for influencing heat transfer. It can also be observed from Table 4 that increase in height significantly increase retention of argon atoms inside of the pores. From quantitative perspective, about 43.7% and 97.0% more argon atoms are found to be adsorbed on the porous substrate at the end of evaporation compared to the flat substrate for void fraction ( $\phi$ ) 41% and 20% respectively at  $\lambda = 0.98$ . For increase in the height of nano-pores, for example, for single and four pore nano substrates at  $\lambda = 2.1$ , about 97% and 90% more argon atoms have been adsorbed with respect to flat surface that is almost double and triple of their respective cases with  $\lambda = 0.98$ . Argon retention inside the pores create a barrier in transferring heat from the walls of porous substrate to the liquid argon, thus it offsets the effect of higher heat transfer area as evident in the present analysis. However, retention might become dominant if the height of the porous substrate is increased too much.

## 4. Conclusion

Molecular Dynamics simulation of thin film evaporation of liquid argon over hexagonal nano-porous substrate has been performed

**Table 3**  
Average wall heat flux for different nano porous substrates.

Void Fraction, $\phi(\%)$	Height to arm thickness ratio, $\lambda$	Average wall heat flux, $q_{w,avg}$ , MW/m <sup>2</sup>
Flat Substrate		488
41%	0.98	718
	1.5	909
	2	1027
	0.98	767
34%	1.5	997
	2	1073
	0.98	771
27%	1.5	1031
	2	1108
	0.98	824
20%	1.5	1075
	2	1177
	0.98	

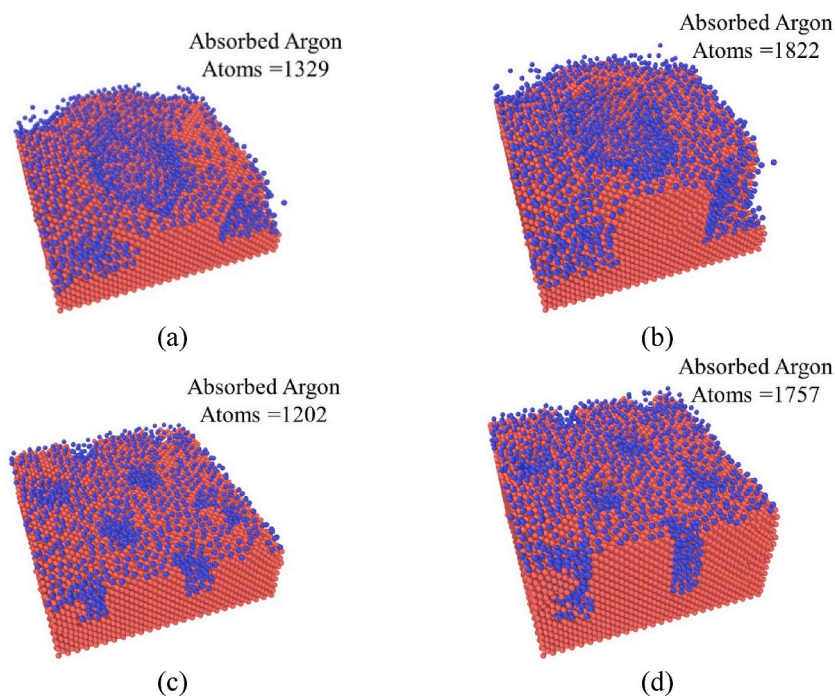


**Fig. 16.** Snapshot of absorbed Argon atoms over nano porous substrate at the end of simulation (6 ns) for (a)  $\phi = 41\%$ ,  $\lambda = 0.98$ ; (b)  $\phi = 41\%$ ,  $\lambda = 2$ ; (c)  $\phi = 20\%$ ,  $\lambda = 0.98$ ; (d)  $\phi = 20\%$ ,  $\lambda = 2$ .

**Table 4**

Comparison of absorption characteristics of different nano porous substrates.

Void Fraction, $\phi$	Height to arm thickness ratio, $\lambda$	Number of argon atoms in pores after evaporation ceases
41%	0.98	1329
	2	1822
20%	0.98	1202
	2	1757

in the present study. Twelve different nano-porous substrates have been modeled considering the variation of void fraction, no. of nano-pores as well as height of the nano-pores. Following necessary equilibration of the atomic system, non-equilibrium heating of thin film liquid argon is done by placing the liquid layer over the porous-substrate and the consequent liquid-vapor phase change characteristics has been observed to reveal out the effect of void fraction and height of the nano-porous substrate. Heat transfer performance of the system has been qualitatively analyzed by observing temperature history of argon and net evaporation number while that has been quantitatively evaluated in terms of time average wall heat flux, average evaporative mass flux and diffusion coefficient of argon. Significant increase in heat transfer is observed for nano porous substrate with lower  $\phi$  and with increasing height of nanopores. Wall heat flux increases by 47.1% and 68.8% compared to flat surface due to the introduction of single and four-pore substrate with a characteristic height to arm thickness ratio ( $\lambda$ ) of 0.98 of the porous substrates. Retention tendency of argon atoms inside the nano-pores significantly increases with the presence of nano-pores as well as the increasing height of the nano-pores. In comparison to flat surface, there was an increase of 43.7% and 30% in the number of argon atoms adsorbed on the porous substrate following the evaporation for the characteristic height to arm thickness ratio of 0.98 of the porous substrates having a void fraction of 41% and 20% respectively. Evaporation has been found to take place faster over nano-porous substrate with lower void fraction which is observed quantitatively with four nano-pore substrates having higher average heat and evaporative mass flux, as well as diffusion coefficient. Insights from this study indicates lower void fraction and more nanopores is better for heat transfer enhancement which will help engineer create better and optimized nano porous substrates used in various applications. However, experimental validation of these insights remains a limitation of this study. Also, other shapes and orientation of nano pores and the optimized height of the nano pores can be investigated in future studies.

#### Author contribution statement

Md. Aminul Islam: Performed the experiments; Analyzed and interpreted the data; Contributed reagents, materials, analysis tools or data; Wrote the paper. Monoranjan Debnath Rony: Performed the experiments; Analyzed and interpreted the data; Contributed

reagents, materials, analysis tools or data; Wrote the paper. Mohammad Nasim Hasan: Conceived and designed the experiments; Analyzed and interpreted the data; Contributed reagents, materials, analysis tools or data; Wrote the paper.

## Acknowledgements

The authors are thankful to Department of Mechanical Engineering, Bangladesh University of Engineering and Technology (BUET), Dhaka, Bangladesh, for providing continuous support in conducting the present research. Authors sincerely acknowledge Basic Research Grant: Grant No.: 5336(100)-Sl. 23; Dated: June 30, 2021; awarded by Bangladesh University of Engineering and Technology (BUET).

## References

- [1] A. Bar-Cohen, P. Wang, E. Rahim, Thermal management of high heat flux nanoelectronic chips, *Microgravity Sci. Technol.* 19 (2007) 48–52, <https://doi.org/10.1007/BF02915748>.
- [2] O.A. Kabov, E.Ya Gatapova, D.V. Zaitsev, Cooling technique based on evaporation of thin and ultra thin liquid films, in: 2008 11th Intersoc. Conf. Therm. Thermomechanical Phenom. Electron. Syst., 2008, pp. 520–527, <https://doi.org/10.1109/ITHERM.2008.4544312>.
- [3] D.G. Cahill, P.V. Braun, G. Chen, D.R. Clarke, S. Fan, K.E. Goodson, P. Keblinski, W.P. King, G.D. Mahan, A. Majumdar, H.J. Maris, S.R. Phillpot, E. Pop, L. Shi, Nanoscale thermal transport. II. 2003–2012, *Appl. Phys. Rev.* 1 (2014), 011305, <https://doi.org/10.1063/1.4832615>.
- [4] C. Ding, G. Soni, P. Bozorgi, B.D. Piorek, C.D. Meinhart, N.C. MacDonald, A flat heat pipe architecture based on nanostructured titania, *J. Microelectromech. Syst.* 19 (2010) 878–884, <https://doi.org/10.1109/JMEMS.2010.2051019>.
- [5] R.K. Cavin, V.V. Zhirnov, D.J.C. Herr, A. Avila, J. Hutchby, Research directions and challenges in nanoelectronics, *J. Nanoparticle Res.* 8 (2006) 841–858, <https://doi.org/10.1007/s11051-006-9123-4>.
- [6] R. Bhardwaj, X. Fang, D. Attinger, Pattern formation during the evaporation of a colloidal nanoliter drop: a numerical and experimental study, *New J. Phys.* 11 (2009), 075020, <https://doi.org/10.1088/1367-2630/11/7/075020>.
- [7] P.L. Woodfield, M. Monde, A.K. Mozumder, Observations of high temperature impinging-jet boiling phenomena, *Int. J. Heat Mass Tran.* 48 (2005) 2032–2041, <https://doi.org/10.1016/j.ijheatmasstransfer.2004.12.011>.
- [8] Md.A. Islam, M. Monde, P.L. Woodfield, Y. Mitsutake, Jet impingement quenching phenomena for hot surfaces well above the limiting temperature for solid–liquid contact, *Int. J. Heat Mass Tran.* 51 (2008) 1226–1237, <https://doi.org/10.1016/j.ijheatmasstransfer.2007.01.059>.
- [9] G. Nagayama, M. Kawagoe, T. Tsuruta, Molecular Dynamics Simulations of Interfacial Heat and Mass Transfer at Nanostructured Surface, American Society of Mechanical Engineers Digital Collection, 2009, pp. 871–880, <https://doi.org/10.1115/MNC2007-21410>.
- [10] K.-H. Chu, R. Enright, E.N. Wang, Structured surfaces for enhanced pool boiling heat transfer, *Appl. Phys. Lett.* 100 (2012), 241603, <https://doi.org/10.1063/1.4724190>.
- [11] T.-B. Nguyen, D. Liu, M.I. Kayes, B. Wang, N. Rashin, P.W. Leu, T. Tran, Critical heat flux enhancement in pool boiling through increased rewetting on nanopillar array surfaces, *Sci. Rep.* 8 (2018) 4815, <https://doi.org/10.1038/s41598-018-22693-z>.
- [12] J. Chen, S. Ahmad, J. Cai, H. Liu, K.T. Lau, J. Zhao, Latest progress on nanotechnology aided boiling heat transfer enhancement: a review, *Energy* 215 (2021), 119114, <https://doi.org/10.1016/j.energy.2020.119114>.
- [13] S. Mori, K. Okuyama, Enhancement of the critical heat flux in saturated pool boiling using honeycomb porous media, *Int. J. Multiphas. Flow* 35 (2009) 946–951, <https://doi.org/10.1016/j.ijmultiphaseflow.2009.05.003>.
- [14] S.A. Khan, N. Sezer, M. Koc, Design, fabrication and nucleate pool-boiling heat transfer performance of hybrid micro-nano scale 2-D modulated porous surfaces, *Appl. Therm. Eng.* 153 (2019) 168–180, <https://doi.org/10.1016/j.applthermaleng.2019.02.133>.
- [15] C. Li, G.P. Peterson, Evaporation/boiling in thin capillary wicks (II)—effects of volumetric porosity and mesh size, *J. Heat Tran.* 128 (2006) 1320–1328, <https://doi.org/10.1115/1.2349508>.
- [16] S. Zhang, X. Jiang, Y. Li, G. Chen, Y. Sun, Y. Tang, C. Pan, Extraordinary boiling enhancement through micro-chimney effects in gradient porous micromeshes for high-power applications, *Energy Convers. Manag.* 209 (2020), 112665, <https://doi.org/10.1016/j.enconman.2020.112665>.
- [17] R. Wen, S. Xu, Y.-C. Lee, R. Yang, Capillary-driven liquid film boiling heat transfer on hybrid mesh wicking structures, *Nano Energy* 51 (2018) 373–382, <https://doi.org/10.1016/j.nanoen.2018.06.063>.
- [18] X. Dai, F. Yang, R. Yang, Y.-C. Lee, C. Li, Micromembrane-enhanced capillary evaporation, *Int. J. Heat Mass Tran.* 64 (2013) 1101–1108, <https://doi.org/10.1016/j.ijheatmasstransfer.2013.05.030>.
- [19] A. Biswas, I.S. Bayer, A.S. Biris, T. Wang, E. Dervishi, F. Faupel, Advances in top–down and bottom–up surface nanofabrication: techniques, applications & future prospects, *Adv. Colloid Interface Sci.* 170 (2012) 2–27, <https://doi.org/10.1016/j.cis.2011.11.001>.
- [20] V.V. Chaban, O.V. Prezhdo, Ab initio molecular dynamics of dimerization and clustering in alkali metal vapors, *J. Phys. Chem.* 120 (2016) 4302–4306, <https://doi.org/10.1021/acs.jpca.6b04609>.
- [21] V.V. Chaban, O.V. Prezhdo, Ionic vapor: what does it consist of? *J. Phys. Chem. Lett.* 3 (2012) 1657–1662, <https://doi.org/10.1021/jz300405q>.
- [22] V.V. Chaban, O.V. Prezhdo, Ionic vapor composition in pyridinium-based ionic liquids, *J. Phys. Chem. B* 120 (2016) 4661–4667, <https://doi.org/10.1021/acs.jpcc.6b03130>.
- [23] H. Liu, X. Qin, S. Ahmad, Q. Tong, J. Zhao, Molecular dynamics study about the effects of random surface roughness on nanoscale boiling process, *Int. J. Heat Mass Tran.* 145 (2019), 118799, <https://doi.org/10.1016/j.ijheatmasstransfer.2019.118799>.
- [24] W. Wang, H. Zhang, C. Tian, X. Meng, Numerical experiments on evaporation and explosive boiling of ultra-thin liquid argon film on aluminum nanostructure substrate, *Nanoscale Res. Lett.* 10 (2015) 158, <https://doi.org/10.1186/s11671-015-0830-6>.
- [25] T. Fu, Y. Mao, Y. Tang, Y. Zhang, W. Yuan, Effect of nanostructure on rapid boiling of water on a hot copper plate: a molecular dynamics study, *Heat Mass Tran.* 52 (2016) 1469–1478, <https://doi.org/10.1007/s00231-015-1668-2>.
- [26] Q. Cao, Z. Cui, Molecular dynamics simulations of the effects of surface sinusoidal nanostructures on nanoscale liquid film phase-change, *J. Therm. Sci.* 29 (2020) 1076–1084, <https://doi.org/10.1007/s11630-019-1152-2>.
- [27] H. Liu, S. Ahmad, J. Chen, J. Zhao, Molecular dynamics study of the nanoscale boiling heat transfer process on nanostructured surfaces, *Int. Commun. Heat Mass Tran.* 119 (2020), 104963, <https://doi.org/10.1016/j.icheatmasstransfer.2020.104963>.
- [28] S.M. Shavik, M.N. Hasan, A.K.M. Monjur Morshed, Molecular dynamics study on explosive boiling of thin liquid argon film on nanostructured surface under different wetting conditions, *J. Electron. Packag.* 138 (2016), <https://doi.org/10.1115/1.4032463>.
- [29] H. Hu, Y. Sun, Effect of nanostructures on heat transfer coefficient of an evaporating meniscus, *Int. J. Heat Mass Tran.* 101 (2016) 878–885, <https://doi.org/10.1016/j.ijheatmasstransfer.2016.05.092>.
- [30] P. Bai, L. Zhou, X. Du, Effects of surface temperature and wettability on explosive boiling of nanoscale water film over copper plate, *Int. J. Heat Mass Tran.* 162 (2020), 120375, <https://doi.org/10.1016/j.ijheatmasstransfer.2020.120375>.
- [31] P. Bai, L. Zhou, X. Du, Effects of liquid film thickness and surface roughness ratio on rapid boiling of water over copper plates, *Int. Commun. Heat Mass Tran.* 120 (2021), 105036, <https://doi.org/10.1016/j.icheatmasstransfer.2020.105036>.
- [32] S. Ahmad, W. Deng, H. Liu, S. Ali Khan, J. Chen, J. Zhao, Molecular dynamics simulations of nanoscale boiling on mesh-covered surfaces, *Appl. Therm. Eng.* 195 (2021), 117183, <https://doi.org/10.1016/j.applthermaleng.2021.117183>.

- [33] R. Diaz, Z. Guo, A molecular dynamics study of phobic/philic nano-patterning on pool boiling heat transfer, *Heat Mass Tran.* 53 (2017) 1061–1071, <https://doi.org/10.1007/s00231-016-1878-2>.
- [34] J.B. Adams, S.M. Foiles, W.G. Wolfer, Self-diffusion and impurity diffusion of fcc metals using the five-frequency model and the Embedded Atom Method, *J. Mater. Res.* 4 (1989) 102–112, <https://doi.org/10.1557/JMR.1989.0102>.
- [35] B.-J. Lee, J.-H. Shim, M.I. Baskes, Semiempirical atomic potentials for the fcc metals Cu, Ag, Au, Ni, Pd, Pt, Al, and Pb based on first and second nearest-neighbor modified embedded atom method, *Phys. Rev. B* 68 (2003), 144112, <https://doi.org/10.1103/PhysRevB.68.144112>.
- [36] A. Hens, R. Agarwal, G. Biswas, Nanoscale study of boiling and evaporation in a liquid Ar film on a Pt heater using molecular dynamics simulation, *Int. J. Heat Mass Tran.* 71 (2014) 303–312, <https://doi.org/10.1016/j.ijheatmasstransfer.2013.12.032>.
- [37] Y. Chen, Y. Zou, Y. Wang, D. Han, B. Yu, Bubble nucleation on various surfaces with inhomogeneous interface wettability based on molecular dynamics simulation, *Int. Commun. Heat Mass Tran.* 98 (2018) 135–142, <https://doi.org/10.1016/j.icheatmasstransfer.2018.08.017>.
- [38] J. Yu, H. Wang, A molecular dynamics investigation on evaporation of thin liquid films, *Int. J. Heat Mass Tran.* 55 (2012) 1218–1225, <https://doi.org/10.1016/j.ijheatmasstransfer.2011.09.035>.
- [39] M.N. Hasan, S.M. Shavik, K.M. Mukut, K.F. Rabbi, A.H.M. Faisal, Atomistic modelling of thin film argon evaporation over different solid surfaces at different wetting conditions, *Micro & Nano Lett.* 13 (2018) 351–356, <https://doi.org/10.1049/mnl.2017.0198>.
- [40] S. Plimpton, Fast Parallel algorithms for short-range molecular dynamics, *J. Comput. Phys.* 117 (1995) 1–19, <https://doi.org/10.1006/jcph.1995.1039>.
- [41] A. Stukowski, Visualization and analysis of atomistic simulation data with OVITO—the Open Visualization Tool, *Model. Simulat. Mater. Sci. Eng.* 18 (2009), 015012, <https://doi.org/10.1088/0965-0393/18/1/015012>.
- [42] M.J. Terry, J.T. Lynch, M. Bunclark, K.R. Mansell, L.A.K. Staveley, The densities of liquid argon, krypton xenon, oxygen, nitrogen, carbon monoxide methane, and carbon tetrafluoride along the orthobaric liquid curve, *J. Chem. Thermodyn.* 1 (1969) 413–424, [https://doi.org/10.1016/0021-9614\(69\)90072-X](https://doi.org/10.1016/0021-9614(69)90072-X).
- [43] H.R. Seyf, Y. Zhang, Effect of nanotextured array of conical features on explosive boiling over a flat substrate: a nonequilibrium molecular dynamics study, *Int. J. Heat Mass Tran.* 66 (2013) 613–624, <https://doi.org/10.1016/j.ijheatmasstransfer.2013.07.025>.
- [44] T. Fu, Y. Mao, Y. Tang, Y. Zhang, W. Yuan, Molecular dynamics simulation on rapid boiling of thin water films on cone-shaped nanostructure surfaces, *Nanoscale Microscale Thermophys. Eng.* 19 (2015) 17–30, <https://doi.org/10.1080/15567265.2014.991480>.
- [45] S. Sarkar, R.P. Selvam, Molecular dynamics simulation of effective thermal conductivity and study of enhanced thermal transport mechanism in nanofluids, *J. Appl. Phys.* 102 (2007), 074302, <https://doi.org/10.1063/1.2785009>.
- [46] W. Wang, S. Huang, X. Luo, MD simulation on nano-scale heat transfer mechanism of sub-cooled boiling on nano-structured surface, *Int. J. Heat Mass Tran.* 100 (2016) 276–286, <https://doi.org/10.1016/j.ijheatmasstransfer.2016.04.018>.